ChemComm
Chemical Communications

Accepted Manuscript

This article can be cited before page numbers have been issued, to do this please use: M. Wang, X. Hu, B. Zuo, S. Huang, X. Chen and H. Yang, *Chem. Commun.*, 2020, DOI: 10.1039/D0CC02823A.

ROYAL SOCIETY OF CHEMISTRY

rsc.li/chemcomm

View Article Online
DOI: 10.1039/D0CC02823A

COMMUNICATION

Liquid Crystal Elastomer Actuator with Serpentine Locomotion

Received 00th January 20xx,
Accepted 00th January 20xx

DOI: 10.1039/x0xx00000x

Meng Wang, Xin-Bao Hu, Bo Zuo, Shuai Huang, Xu-Man Chen and Hong Yang*

A snake-mimic soft actuator composed of a bilayered liquid crystal elastomer ribbon and two serrated feet is reported in this work. Under repeating on/off near-infrared light irradiation, this actuator can move forward relying on a reversible shape morphing between S-curve structure and reverse S-curve structure, which is similar to the serpentine locomotion of snakes.

Soft-bodied animals, such as octopuses, worms and snakes, can regularly deform their shapes to realize efficient locomotion to adapt to different natural environments, which have attracted scientific attentions in developing a series of bionic soft actuators,[1-10] such as caterpillar-like walking robots,[11-14] flytrap mimics,[15] octopus-inspired robots,[16,17] etc. As the representative soft-bodied reptile, snake has four basic locomotion modes: serpentine, sidewinding, caterpillar and concertina.[18,19] Among them, serpentine locomotion is an S-curve movement, which can be simplified into a reversible shape morphing between S-shaped structure and reverse S-shaped structure, as shown in Fig. 1a. In such a locomotion mode, snake contracts its muscles, thrusts its body from side to side, and creates a series of S-shaped curves, which generate asymmetrical friction force between the ventral scales and the rough ground, and further propel the snake forward. Although some previously synthesized actuators have mimicked the sidewinding,[20,21] concertina[22] and caterpillar[22] motions, there were barely any reports of snake-like soft actuators focusing on serpentine locomotion.

The key challenge in the fabrication of serpentine-type soft actuators is how to achieve a reversible transformation from one S-shaped motion to the reverse S-shaped motion. Here we report our effort on synthesizing a snake-mimic soft actuator with serpentine locomotion, by using liquid crystal elastomer (LCE) which as a classical kind of two-way shape memory material, can reversibly undergo a large shape deformation from one permanent state to anther permanent state induced by the LC-to-isotropic phase transition and have widespread applications in soft actuators.[23-39] To allow such a snake-mimic device to achieve the desired serpentine locomotion, the LCE-based soft actuator should have one S-shaped structure in one permanent state (State 1) and the reverse S-shaped structure in another permanent state (State 2). Under the on-off application of external stimuli, this LCE actuator will reversibly and repeatedly deform from permanent state 1 to permanent state 2, to simulate the serpentine locomotion as shown in Fig. 1b.

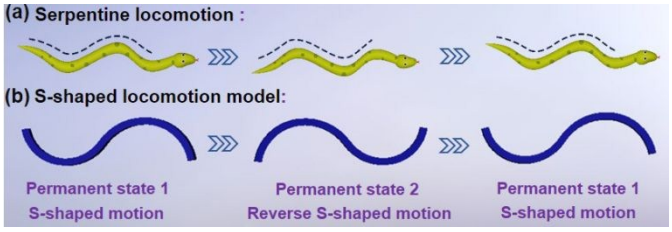

Fig. 1 (a) Cartoon illustration of the serpentine locomotion of snakes. (b) Schematic diagram of the S-shaped locomotion model.

Based on this basic design logic, two strategies were adopted to fabricate snake-mimic soft actuators. The first strategy as shown in Fig. 2a, was very straightforward, we built an S-shaped structure (State 1) in the polydomain LCE sample obtained from the pre-crosslinking stage, performed mechanical programming to reverse the S-shaped structure, and solidified this permanent state 2 during the second crosslinking stage. Meanwhile, in order to achieve a remote control of the actuators, we endowed the LCE sample with photo-thermal conversion effect so that a light stimulus would trigger the LC-to-isotropic phase transition and the consequent shape morphing between two permanent states.

According to strategy 1, we tried several LCE systems, including polysiloxane LCEs,[40,41] polyacrylate LCEs[42] and thiol-ene LCEs,[43,44] which all failed in providing wave-shaped pre-crosslinked LCE samples in a wavy-bottom mould, possibly due to the low viscosities of these LCE systems. Alternatively, a two-step acyclic diene metathesis (ADMET) *in-situ* polymerization/crosslinking approach[45] successfully prepared a single-layered S-shaped LCE film, named as **LCE0** (1.3 cm long × 0.27 cm wide, the thickness was ca. 180 μm). The detailed

School of Chemistry and Chemical Engineering, Jiangsu Province Hi-Tech Key Laboratory for Bio-medical Research, State Key Laboratory of Bioelectronics, Institute of Advanced Materials, Southeast University, Nanjing, 211189, China. E-mail: yangh@seu.edu.cn

† Footnotes relating to the title and/or authors should appear here.
Electronic Supplementary Information (ESI) available: [details of any supplementary information available should be included here]. See DOI: 10.1039/x0xx00000x

fabrication protocol is described in the supporting information. Under NIR light irradiation, this S-shaped LCE ribbon exhibited a reversible deformation from the wavy structure (state 2) to a nearly flat state instead of the desired reverse wavy structure (state 1). There are two possible reasons for this compromised result: (1) due to gravity, the thickness of the LCE film prepared at the pre-crosslinking stage was inhomogeneous; (2) the shape of the LCE sample at the isotropic state deviated largely from the one of its polydomain mesogenic state (state 1).

We further optimized the strategy 1, by adopting one extra LCE supporting layer which had larger contraction strain than the main LCE layer and would contribute to reverse the S-shaped structure beyond the LC-to-isotropic phase transition. Following this second strategy, we synthesized a dual-layer, dual-composition LCE film. This bilayered LCE film was consisted of one main layer and two other outer layers stuck on the ridge sides of the main layer. The preparation protocols of the main layer **LCE1**, the outer layer **LCE2** and the bilayered LCE ribbon are schematically illustrated in Fig. 2b. For **LCE1**, a thiol-acrylate LC mixture[44] containing the nematic monomer 1,4-bis-[4-(3-acryloyloxypropyloxy)benzoyloxy]-2-methylbenzene (**RM257**), the chain extender 1,2-bis(2-mercaptoethoxy)ethane(**DODT**), the crosslinker pentaerythritol tetra(3-mercaptopropionate) (**PETMP**), the photoinitiator **Irgacure 651** and dipropylamine (**DPA**) catalyst (Formula 2, Fig. 2c), was poured into a flat-bottom PTFE mould to go through the pre-crosslinking stage.[44] After removing from the mould, the obtained flat film was cut into thin strips. The flat strip was then pressed between two intermeshing wave-shaped transparent glass moulds to form the wavy structure. After polymerization under 365 nm ultraviolet (UV) light for 5 min, a wavy film was removed from the mould and cut into an S-shaped ribbon **LCE1** (1.3 cm long × 0.27cm wide, the thickness was ca. 640 μm). The outer layer **LCE2** (0.65 cm long × 0.27 cm wide, the thickness was ca. 120 μm) was the ADMET LCE system based on formula 1.[45] Different from the preparation protocol of **LCE1**, the mechanical programming of **LCE2** would have an extra uniaxial-stretching treatment before the curve-shape model-pressing, so that **LCE2** would have a much larger contraction strain than **LCE1**. Eventually, the bilayered LCE ribbon was obtained by gluing two arc-shaped **LCE2** strips on the two opposite ridge sides of the S-shaped **LEC1** film. In such a design, when the temperature was raised to above the clearing point, the bilayered LCE ribbon would bend towards the more contracted **LCE2** layers, forcing the ridge sides to become the corrie sides, so that the original S-shaped structure would turn to reverse S-curve.

To investigate the optical absorption property of the bilayered LCE ribbon, the ultraviolet-visible (UV-vis) absorption spectra of the NIR-absorbing dye **YHD796C**, **LCE1** and **LCE2** strips were recorded by a TU-2700 UV-Vis spectrophotometer. As shown in Fig. 3a and Fig. S2, all the samples had a main absorption peak in the NIR absorption region centered at 796 nm, which indicated that the two LCE strips were both sensitive to NIR light. The photothermal conversion capacities of the two

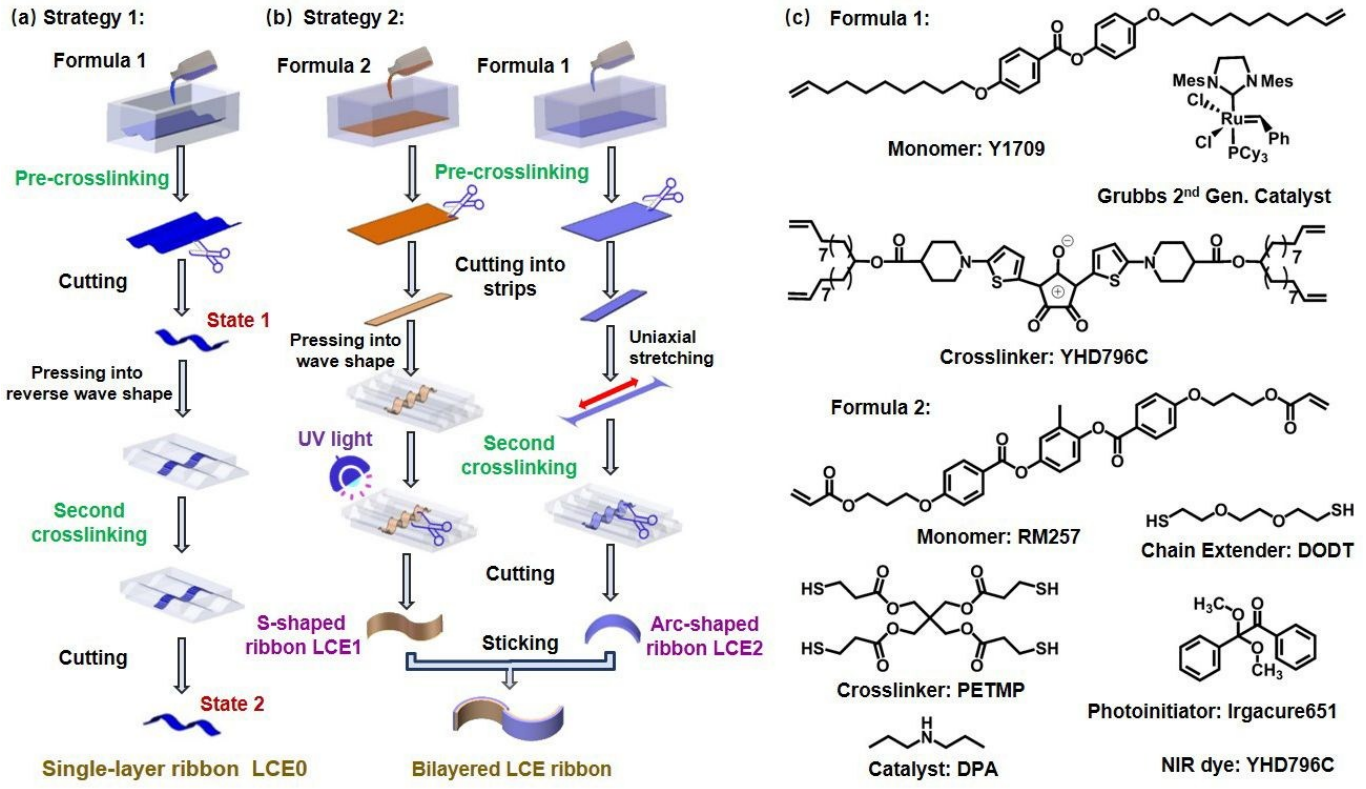

Fig. 2 Schematic illustration of the fabrication protocols based on (a) strategy 1 and (b) strategy 2. (c) The chemical compositions of the ADMET LCE system (Formula 1) and the thiol-acrylate LCE system (Formula 2) used in this work.

View Article Online
DOI: 10.1039/D0CC02825A

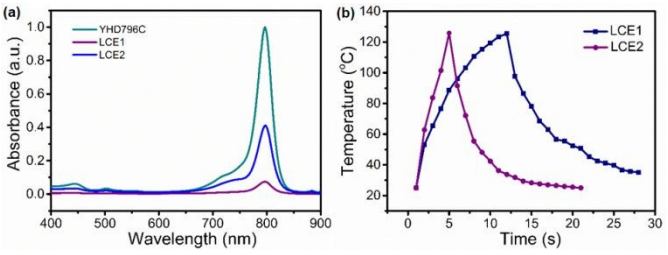

Fig. 3 (a) UV–vis spectra of YHD796C, **LCE1** and **LCE2** samples (conc = 0.15 mg/ml) dispersed in CH_2Cl_2. (b) Temperature profiles of **LCE1** and **LCE2** samples, irradiated by 808 nm NIR light.

LCE samples were further studied by a thermal imager. As shown in Fig. 3b, after irradiated under 808 nm NIR light for 4 s, Under the same irradiation condition, the surface temperature of the **LCE1** strip could reach to 70 °C in the first 4 s, which was higher than its T_{iso} (65.2 °C, Fig. S1a), and continue to rise to 125 °C in 10 s. When NIR-light was removed, the temperature of the temperature in the next 20 s. The mechanical properties of the two LCE samples were measured by a dynamic mechanical analyzer (DMA Q850, TA instrument). As shown in Fig. S3, beyond the LC-to-isotropic phase transition temperature, the elastic modulus of the supporting layer **LCE2** (e.g. 1.3 MPa, 135 °C) was much higher than the modulus of the main layer **LCE1** (e.g. 0.3 MPa, 80 °C), which would help the supporting LCE layer to reverse the S-shaped structure of the main LCE layer.

Encouraged by the above results, we fabricated a NIR light-driven snake-mimic actuator, as schematically illustrated in Fig. 4a. The snake-mimic robot consisted of an S-shaped bilayered LCE ribbon and two serrated feet attached onto the front and back ends of the LCE ribbon. The support feet with inclined serrations[5,11] could not only provide asymmetric friction force for the serpentine robot, but also make the ribbon actuator always stand on the ground in a side vertical manner during locomotion. As shown in Fig. 4b,c and Video S1, this S-shaped actuator constantly deformed between an S-shaped motion and a reverse S-shaped motion, and moved forward with a crawling velocity of ca. 0.13 mm/s under the repeating on/off illumination cycles of 808 nm light (15 s per cycle, including 9 s light on and 6 s light off), which was similar to the serpentine locomotion of snakes. Meanwhile, it could be observed that the longitudinal body length of the actuator increased first and then decreased to the original length under illumination. The same length change trend could also be recorded after removing the NIR light. During these regular length changing processes, benefitted from the support feet with inclined serrations, the friction force to the left was always greater than that to the right ($f_1 > f_2$),[7,46] so the crawler could always move forward to the right side during the NIR light on/off cycles.

The real-time position coordinate of the point A of the S-shaped LCE actuator was recorded and plotted in Fig. 4d. Under repeating on/off illumination cycles of 808 nm light, the location distribution of the point A presented a regular forward wave motion trajectory, which indicated that the reversible shape-morphing process and the continuous forward movement of the actuator were simultaneous. To investigate the snake- mimic actuator deforming and moving quantitatively, the curve of the angle α between line l_1 and line l_1 along with the time of NIR light irradiation was plotted in Fig. 4e. Here, l_1 and l_2 were tangents to the left end point and the left arc midpoint of the bilayered LCE ribbon, respectively. It could be seen that the angle α quickly changed from 72° to -45° in 9 s, implying the accomplishment of the first deformation from an S-curve to a reverse S-curve. After the removal of NIR light, the angle α recovered to 72° in the next 6 s, owing to the recovery of crawler from the reverse S-shaped motion to the original S-shaped motion. According to the curvature radius formula: $1/r = (\alpha \times \pi \div 180) \div l$, where l was the length of the half left arc, the corresponding curve of the bending curvature ($1/r$) with irradiation time was further plotted in Fig. 4f. Similarly, the curvature changed between 3.14 cm^{-1} and -2.0 cm^{-1} in a stimulation cycle composed of 9 s light on and 6 s light off. The change of data from positive to negative sign indicated the inversion of the S-shaped motion. In the next four irradiation cycles, the changes of angle and curvature were consistent with those of the first cycle, which indicated that the crawler could keep moving forward through a regular morphing between the S-shaped motion and the reverse S-shaped motion.

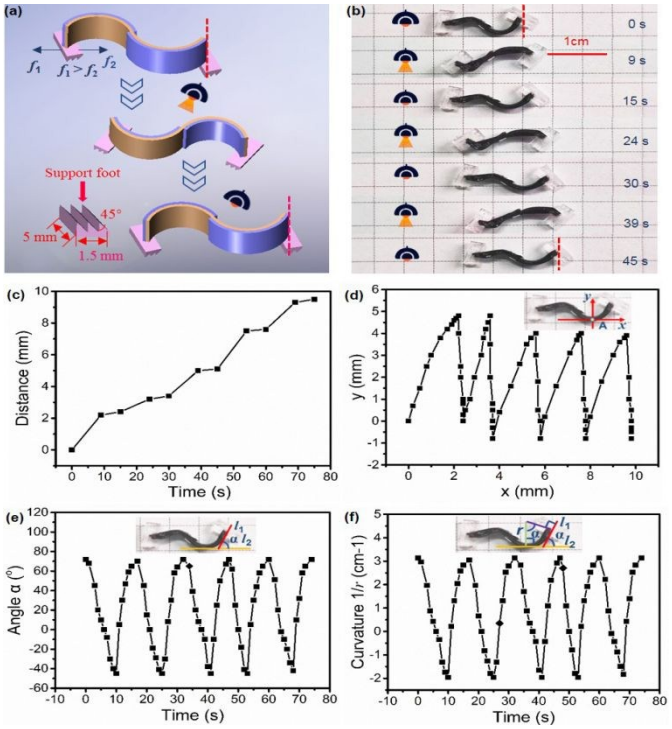

Fig. 4 (a) Schematic illustration of a snake-mimic soft actuator. (b) The images of the serpentine robot moving under the repeating on/off illumination cycles of 808 nm light. (c) The time-dependent motion distance of the snake-mimic actuator. (d) The real-time position coordinate of the point A of the S-shaped LCE actuator. (e) The included angle

α vs NIR light illumination time diagram of the LCE actuator. (f) Curvature (1/*r*) as a function of NIR light illumination time of the LCE actuator.

In summary, a novel snake-mimic actuator composed of a bilayered LCE ribbon and two serrated feet was designed and fabricated in this work. The LCE actuator could realize a reversible deformation from an S-shaped motion to a reverse S-shaped motion caused by the different shape deformation behaviours of the two LCE layers. Moreover, under repeating on/off NIR light irradiation, this crawler robot could move forward relying on the asymmetric friction, which was similar to the serpentine locomotion of snakes. We hope that this NIR-fuelled serpentine-type LCE robot would provide a new perspective for fabrication and development of bio-mimic soft actuator devices.

This research was supported by National Natural Science Foundation of China (No.21971037, 51903048), Jiangsu Provincial Natural Science Foundation of China (No. BK20170024, BK20180406), and the Fundamental Research Funds for the Central Universities (No. 2242020K40034). We thank Dr. Hao Zeng (Tampere University of Technology, E-mail: hao.zeng@tut.fi) for helpful scientific discussions.

Conflicts of interest

There are no conflicts of interest to declare.

Notes and references

1 D. Rus and M. T. Tolley, *Nature*, 2015, **521**, 467-475.
2 L. Hines, K. Petersen, G. Z. Lum and M. Sitti, *Adv. Mater.*, 2017, **29**, 1603483.
3 H. Lin, G. Leisk and B. Trimmer, *Acta Futura*, 2013, **6**, 69-79.
4 H. Yuk, S. T. Lin, C. Ma, M. Takaffoli, N. X. Fang and X. H. Zhao, *Nat. Commun.*, 2017, **8**, 14230.
5 H. Zeng, P. Wasylczyk, D. S. Wiersma and A. Priimag, *Adv. Mater.*, 2018, **30**, 1703554.
6 Y. Y. Xiao, Z. C. Jiang, X. Tong and Y. Zhao, *Adv. Mater.*, 2019, **31,** 1903452.
7 C. Ahn, X. D. Liang and S. Q. Cai, *Adv. Mater. Technol.*, 2019, **4**, 1900185.
8 J. Hu, X. Li, Y. Ni, S. Ma and H. Yu, *J. Mater. Chem. C*, 2018, **6**, 10815-10821.
9 N. W. Bartlett, M. T. Tolley, J. T. Overvelde, J. C. Weaver, B. Mosadegh, K. Bertoldi, G. M. Whitesides and R. J. Wood, *Science*, 2015, **349**, 161-165.
10 Y. Bahramzadeh and M. Shahinpoor, *Soft Robot*, 2014, **1**, 38-52.
11 L.Y. Sun, Z.Y. Chen, F. K. Bian and Y. J. Zhao, *Adv. Funct. Mater.*, 2020, **30**, 1907820.
12 H. J. Lu, M. Zhang, Y. Y. Yang, Q. Huang, T. Fukuda, Z. K. Wang and Y. J. Shen, *Nat. Commun.,* 2018, **9**, 3944.
13 H. Zeng, O. M. Wani, P. Wasylczyk and A. Priimagi, *Macromol. Rapid Commun.*, 2018, **39**, 1700224.
14 C. J. Wang, K. Sim, J. Chen, H. Kim, Z. Y. Rao, Y. H. Li, W. Q. Chen, J. Z. Song, R. Verduzco and C. J. Yu, *Adv. Mater.*, 2018, **30**, 1706695.
15 O. M. Wani, H. Zeng and A. Priimagi, *Nat. Commun.*, 2017, **8**, 15546.
16 M. Wehner, R. L. Truby, D. J. Fitzgerald, B. Mosadegh, G. M. Whitesides, J. A. Lewis and R. J. Wood, *Nature*, 2016, **536**, 451-455.
17 C. Laschi, M. Cianchetti, B. Mazzolai, L. Margheri, M. Follador and P. Dario, *Adv. Robotics*, 2012, **26**, 709-727.
18 M. Saito, M. Fukaya and T. Iwasaki, *IEEE Contr. Syst. Mag.,* 2002, **22**, 64-81.
19 T. Owen, *Robotica*, 1994, **12**, 282-282.
20 H. Marvi, C. H. Gong, N. Gravish, H. Astley, M. Travers, R. L. Hatton, J. R. Mendelson, H. Choset, D. L. Hu and D. I. Goldman, *Science*, 2014, **346**, 224-229.
21 I. Tanev, T. Ray and A. Buller, *IEEE T. Robot.*, 2005, **21**, 632-645.
22 Y. Y. Yang, M. Zhang, D. F. Li and Y. J. Shen, *Adv. Mater. Technol.*, 2019, **4**, 1800366.
23 T. J. White and D. J. Broer, *Nat. Mater.,* 2015, **14,** 1087-1098.
24 B. C. Ohm, M. Brehmer and R. Zentel, *Adv. Mater.*, 2010, **22**, 3366-3387.
25 H. F. Yu and T. Ikeda, *Adv. Mater.*, 2011, **23**, 2149-2180.
26 Z. C. Jiang, Y. Y. Xiao and Y. Zhao, *Adv. Opt. Mater.*, 2019, **7**, 1900262.
27 X. L. Pang, J. A. Lv, C. Y. Zhu, L. Qin and Y. L. Yu, *Adv. Mater.*, 2019, **31**, 1904224.
28 T. H. Ware, M. E. McConney, J. J. Wie, V. P. Tondiglia and T. J. White, *Science*, 2015, **347**, 982-984.
29 A. H. Gelebart, D. J. Mulder, M. Varga, A. Konya, G. Vantomme, E. W. Meijer, R. L. B. Selinger and D. J. Broer, *Nature*, 2017, **546**, 632-638.
30 S. Iamsaard, S. J. Aßhoff, B. Matt, T. Kudernac, J. J. Cornelissen, S. P. Fletcher and N. Katsonis, *Nat. Chem.,* 2014, **6**, 229-235.
31 Z. Q. Pei, Y. Yang, Q. M. Chen, E. M. Terentjev, Y. Wei and Y. Ji, *Nat. Mater.*, 2014, **13**, 36-41.
32 S. V. Ahir, A. R. Tajbakhsh and E. M. Terentjev, *Adv. Funct. Mater.*, 2006, **16**, 556-560.
33 T. Ube, K. Kawasaki and T. Ikeda, *Adv. Mater.,* 2016, **28**, 8212-8217.
34 A. H. Gelebart, D. J. Mulder, G. Vantomme, A. P. H. J. Schenning and D. J. Broer, *Angew. Chem. Int. Ed.* 2017, **56**, 13436-13439.
35 H. Shahsavan, S. M. Salili, A. Jákli and B. X. Zhao, *Adv. Mater.*, 2017, **29**, 1604021.
36 M. K. McBride, A. M. Martinez, L. Cox, M. Alim, K. Childress, M. Beiswinger, M. Podgorski, B. T. Worrell, J. Killgore and C. N. Bowman, *Sci. Adv.,* 2018, **4**, eaat4634.
37 Y. Xia, X. Y. Zhang and S. Yang, *Angew. Chem. Int. Ed.,* 2018, **57**, 5665-5668.
38 A. J. Kragt, D. C. Hoekstra, S. Stallinga, D. J. Broer and A. P. H. J. Schenning, *Adv. Mater.,* 2019, **31**, 1903120.
39 H. Zeng, M. Lahikainen, L. Liu, Z. Ahmed, O. M. Wani, M. Wang, H. Yang and A. Priimagi, *Nat. Commun.,* 2019, **10**, 5057.
40 J. Küpfer and H. Finkelmann, *Makromol. Chem. Rapid Commun.,* 1991, **12**, 717-726.
41 B. Zuo, M. Wang, B. P. Lin and H. Yang, *Nat. Commun.,* 2019, **10**, 4539.
42 A. Buguin, M. H. Li, P. Silberzan, B. Ladoux and P. Keller, *J. Am. Chem. Soc.*, 2006, **128**, 1088-1089.
43 H. Yang, A. Buguin, J. M. Taulemesse, K. Kaneko, S. Méry, A. Bergeret and P. Keller, *J. Am. Chem. Soc.,* 2009, **131**, 15000-15004.
44 C. M. Yakacki, M. Saed, D. P. Nair, T. Gong, S. M. Reed and C. N. Bowman, *Rsc Adv.*, 2015, **5**, 18997-19001.
45 L. Liu, M. H. Liu, L. L. Deng, B. P. Lin and H. Yang, *J. Am. Chem. Soc.*, 2017, **139**, 11333-11336.
46 Q. M. Chen, Y. S. Li, Y. Yang, Y. S. Xu, X. J. Qian, Y. Wei and Y. Ji, *Chem. Sci.*, 2019, **10**, 3025-3030.

View Article Online
DOI: 10.1039/D0CC02823A

Table of Contents Graphic

Liquid Crystal Elastomer Actuator with Serpentine Locomotion

Meng Wang, Xin-Bao Hu, Bo Zuo, Shuai Huang, Xu-Man Chen and Hong Yang*

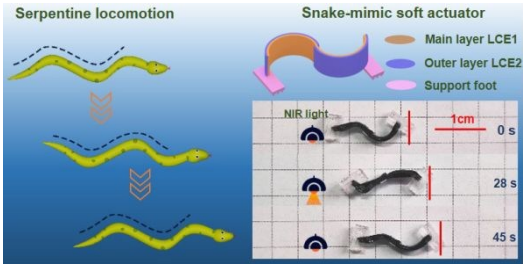

In this manuscript, we describe a snake-mimic soft actuator with serpentine locomotion, which can move forward relying on a reversible shape morphing between S-curve and reverse S-curve structures.